Characterization of the pneumatic behavior of a novel spouted bed apparatus

O. Gryczka[1], S. Heinrich[1], N.G. Deen[2], J.A.M. Kuipers[2] and L. Mörl[1]

1 - Faculty of Process and Systems Engineering, Otto-von-Guericke-University, Magdeburg, Germany
2 – Faculty of Science and Technology, University of Twente, Enschede, The Netherlands

Abstract - Recently the importance of spouted bed technology has significantly increased in the context of drying processes as well as granulation, agglomeration or coating processes. Particulate systems concerning very fine or non spherical particles that are difficult to fluidize, often cannot be treated in conventional fluidized beds. In contrast to those fluidized beds, the spouted bed technology with its specific flow structure offers the opportunity of stable fluidization under controlled conditions. Within this work the fluid dynamics of a novel spouted bed with two adjustable gas inlets is investigated. By analysis of gas fluctuation spectra by means of a fast Fourier transformation algorithm, different operation regimes are identified and depicted graphically. Furthermore, continuum CFD-modeling of the granular solid phase motion by means of an Euler/Euler approach and comparisons with experimental obtained velocity vector fields by means of particle image velocimetry (PIV) measurements will be presented in this work.

INTRODUCTION

In food, pharmaceutical and chemical industry, fine and polydisperse solids are treated and produced, respectively. Analogous to conventional fluidized beds, spouted beds are well known for their good mixing of the solid phase and also for their intensive heat and mass transfer characteristics between the fluid phase (gas) and the solid phase yielding nearly isothermal conditions. The special flow structure of a spouted bed is characterized by a simple apparatus construction. Like the fluidized bed technology, the spouted bed technology can be applied for mixing of particpulate systems, for heat and mass transfer processes, e.g. cooling, drying (Kmiec et al. (1994)), calcination, combustion, gasification as well as for complex multiphase processes like spray granulation (Hatano et al. (2004)), agglomeration (Jacob et al. (2005)), particle layering and coating (Kfuri and Freitas (2005)) and also for chemical reactions. The elementary differences of spouted beds in comparison to conventional fluidized beds are:

- a gradual decrease of the gas velocity over the apparatus height, enabling the treatment of poly-disperse particle systems at different pneumatic operating ranges,
- a sufficient high gas velocity in the bottom part of the apparatus, that allows the treatment of materials where an extended contact with the gas distributor is unallowable,
- high possible gas inlet temperatures. Particles are located in the jet zone for only a short period of time, whereby a high degree of thermal efficiency and high evaporation rates are realized. Also temperature sensitive materials can be treated gently due to much lower gas temperatures outside the jet zone.

Knowledge of the stable fluid dynamic operation range of the spouted bed, which is smaller compared with conventional fluidized beds, is of importance for operating the apparatus. In the recent literature, the pneumatic operation range is depicted with the aid of different diagrams, e.g. ΔP = f(velocity) (Markovski and Kaminski (1983), Olazar et al. (1992)), H_o = f(velocity) (Olazar et al. (1992)), velocity = f(diameter) (Čatipović et al. (1978)) or by Re-G-Ar-diagrams (Mitev (1979), Piskova (2002)). The pneumatic operation ranges of spouted beds are usually characterized in a quantitative manner by analysis of measured gas phase pressure fluctuations and fast Fourier analysis (FFT) on these spectra. Based on the FFT analysis the pneumatic stable operation range will be identified and depicted in a dimensionless Re-G-Ar-diagram similar to the work of Mitev (1979).

Another aspect of this work is modeling the pneumatic behavior of the spouting process with the commercial software package FLUENT 6.2. The aim of the investigations is to predict the pressure drop of the void apparatus as well as the solid phase motion by means of a continuum Euler/Euler approach. In this approach both the fluid phase and the granular solid phase are considered as fully interpenetrating continua. The results obtained by CFD modeling, e.g. solid phase velocity vector fields, are compared with experimental results provided by particle image velocimetry (PIV).

DEVELOPMENT OF A NOVEL SPOUTED BED APPARATUS

The main item of the investigated spouted bed apparatus is the gas distributor which consists of two adjustable chopped cylinders (Mörl et al. (2001), Piskova (2002)). By rotating the cylinders, the free cross section area of the gas inlet can be varied (Fig. 1). Thus, the opening ratio of the gas distributor and consequently

the gas inlet velocity can be regulated directly during the operation. This constitutes an advantage when the gas distributor gets clogged with bed material. By varying the gas inlet area, clogging and dead zones within the apparatus are eliminated without interrupting the process. The fluidization gas is sucked into the apparatus horizontally through the two slits that extend along the whole apparatus depth (see Fig. 1) by a sucking ventilator. After passing the slits, the gas flow is diverted upwards mutually by a center profile. On top of the centre profile, the flows from both sides unite and form a jet which passes the apparatus vertically from the bottom to the top. Due to this region with high gas velocities, process gas is sucked into the jet flow from the upwards extending process chamber (solid arrows in Fig. 1). Thus, a special and clearly defined flow structure is formed in the apparatus, which is characterized by an unequal velocity distribution over the cross section area. In the central region above the centre profile, one or more nozzles can be integrated for supplementary coating or granulation (layering) of particles. These nozzles usually spray liquid into the bed in the upward direction ("bottomspray"). Particles located in the process chamber are entrained upwards by the core jet (dashed arrows in Fig. 1). In the upper process chamber the entrained particles are ejected to the sides and move back towards the gas entry zone. Due to the slope of the inner profile, the particles are transported to the lower area of the gas jet, where they are entrained upwards. Thus, a circulating particle motion is obtained, which is quite uniform and rather well defined. Based on this flow structure, different regions within the apparatus cross section area can be distinguished. The region with high gas velocities above the middle profile is referred to as the "jet zone". A flow structure similar to those experienced in pneumatic conveying can be encountered in that region. The two zones adjacent to the jet zone are called the "back-flow zones". By the patented adjustable gas flow regulation (Mörl et al. (2001)), the throughput of process gas as well as the direction of the entering gas can be influenced selectively. Hence, flow conditions in the bottom region of the "jet zone" can be regulated with respect to the gas velocity and the width of the jet as well as the force exposure on the particles. Particularly, during the development time of applications, this adjustability is an advantage. Compared to conventional conical or conical-cylindrical spouted beds, the scale-up of the prismatic apparatus design can occur just by increasing the apparatus depth or length, because the fluid dynamics of a pseudo-2D spouted bed behaves similar to three the dimensional case.

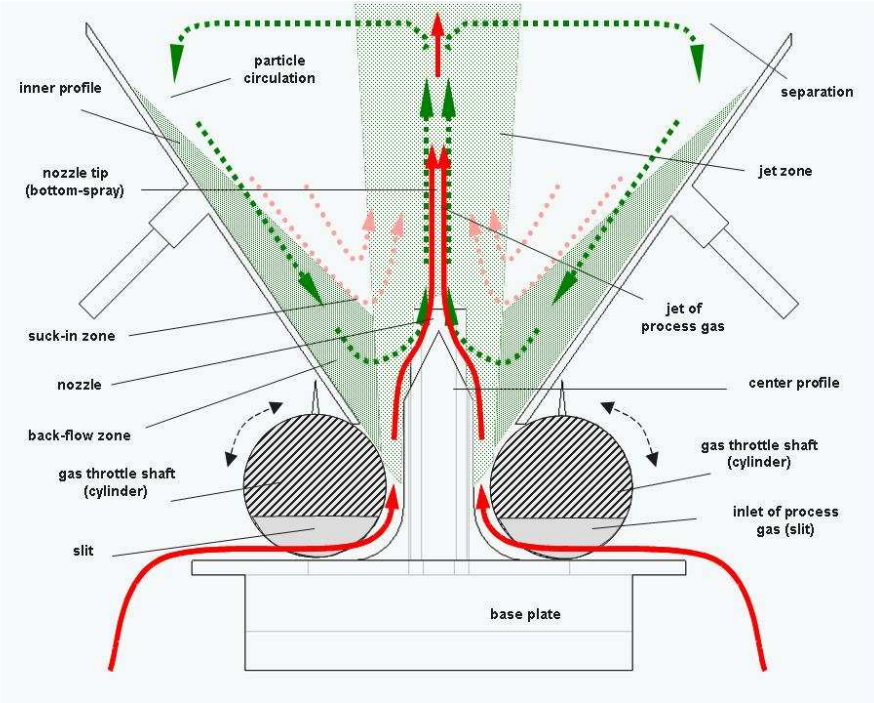

Fig. 1: Schematic of the spouted bed apparatus with slit-shaped adjustable gas inlet.

DETERMINING THE STABLE SPOUTING DOMAIN

Whether the pneumatic operation regime is stable or not depends on the distribution of both phases in the gas-solid spouted bed. Visual observations and FFT analysis on bed pressure drop signals showed that the characteristics of instable operation are channel formation, bubbles and dead zones, whereas the stable operation regime exhibits a good mixing of both phases in the apparatus. The ranges of stable and instable operation can be depicted as a geometric area of operating points which are characterized by different inlet gas velocities, Archimedes-numbers, bed masses and cross section areas of the gas inlet (Kojouharov (2004)). To obtain the boundaries of the stable spouting range, the inlet gas velocity, the bed mass, the free gas entry area and the particle system were varied. As stability criteria for characterization of the pneumatic operation ranges of fluidized beds and spouted beds, Mitev (1979) and Piskova (2002) proposed a dimensionless Re-G-Ar-diagram. At a given gas inlet velocity and particle Archimedes number, a geometric parameter G is defined which describes the ratio between the cross section of the free gas inlet area $A_{gas.inlet}$ and the apparatus cross section area at the bed surface under fixed bed conditions:

$$G = \frac{A_{gas,inlet}}{A_{bed}} \tag{1}$$

For calculation of the parameter G, it is required that the fixed bed height does not exceed the conical apparatus zone. $Re_{inlet,bsf}$ is the Reynolds number in the gas inlet area at the beginning of stable spouting.

$$Re_{inlet,bsf} = \frac{v_{gas} d_s}{\nu_{gas}} \tag{2}$$

The Archimedes number was calculated as following:

$$Ar = \frac{g d_s^3 (\rho_s - \rho_{gas})}{\nu_{gas}^2 \rho_{gas}} \tag{3}$$

More information about the Re-G-Ar diagram can be found in Gryczka et al. (2008). Fig. 2 shows the experimentally obtained overpressure and bed pressure drop values as a function of the gas throughput. At different inlet gas volume flows (points 1 to 14), gas phase pressure fluctuations over the entire bed were measured with a frequency of 1 kHz for a period of 10 seconds and subsequently the fast Fourier transformation algorithm was applied to each of these measured spectra (see the two examples shown at the right hand side of Fig. 2).

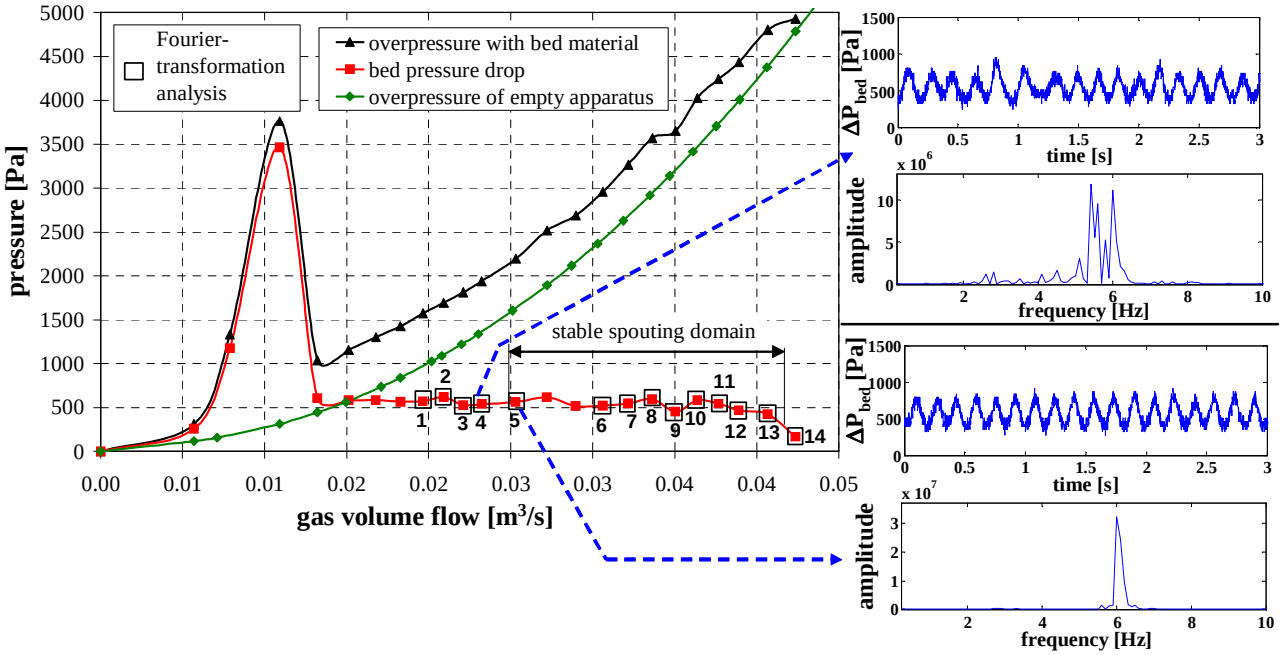

Fig. 2: Measured pressure drop of the empty and filled apparatus and resulting bed pressure drop (material: γ-Al_2O_3 spheres; $d_{50,3}$ = 1.75 mm; σ = 0.048 mm; ρ_s = 1040 kg/m³).

By visual observations and by analysis of the progression of the bed pressure drop as well as of the FFT, conclusions on the dynamic bed behavior can be made and the stable spouting operation range could be determined (exemplary see Fig. 2 for the "stable spouting domain"). Having performed that procedure with several particle systems, bed masses, free inlet gas areas and inlet gas velocities, the stable operation range could be established in the Re-G-Ar-diagram. The stable operation range of the investigated novel spouted bed apparatus with slit-shaped gas inlet has been added to an existing Re-G-Ar-diagram that already implied operation ranges of different other plant constructions (Fig. 3). The curves a, c, e, g and i indicate the beginning of stable operation and the curves b, d, f, h and j the end of stable operation of the corresponding apparatus. The pneumatic operation ranges of the fluidized bed and the several spouted bed designs make comparisons of different apparatus constructions possible and thus facilitate the choice of the optimal apparatus for a certain material. Fig. 3 shows that the stable operation range of the investigated spouted bed apparatus is located at very low G-values affected by very low gas inlet areas. Due to the resulting high inlet gas velocities, excellent heat- and mass transfers are enabled which offer advantages in conducting drying, granulation or coating processes.

CFD MULTIPHASE-MODELING

Another aspect of this work was the CFD-modeling of the hydrodynamics of the spouting process with the continuum two-fluid model (TFM) in the commercial software package FLUENT 6.2. The CFD two-fluid

continuum model is an appropriate tool for modeling engineering-scale fluidized and spouted beds due to the huge number of particles (typically 10^9–10^{12}) present in the system of interest. Several authors applied CFD continuum modeling for fluidized beds (Goldschmidt et al. (2004); van Wachem et al. (1999)) and spouted beds (Kojouharov (2004); Mujumdar et al. (2007)). The conservation equations employed in this continuum model are a generalization of the Navier-Stokes equations for interacting continua. To describe the rheology of the fluidized particles within the continuum model, additional closure laws according to the kinetic theory of granular flow are incorporated. This theory provides explicit closures that take energy dissipation due to non-ideal particle-particle collisions into account by means of the coefficient of restitution. Table 1 shows an overview of the governing equations and the most important simulation settings.

Initially the dependency of the pressure drop of the empty apparatus on the inlet gas volume flow was predicted by means of a standard k-e turbulence model. Fig. 4 shows the comparison between experimental and calculated data. The error bars in Fig. 4 indicate 10% deviation of the calculated curve. A satisfactory agreement of the calculated pressure drop values with experimental results was achieved. Furthermore, the time dependent distribution of the phases in the apparatus as well as velocity vector fields were calculated by the continuum Euler/Euler approach. The simulation results show good resemblance with images taken during experiments. Furthermore, calculated and experimentally obtained particle velocity vector fields by PIV agree well.

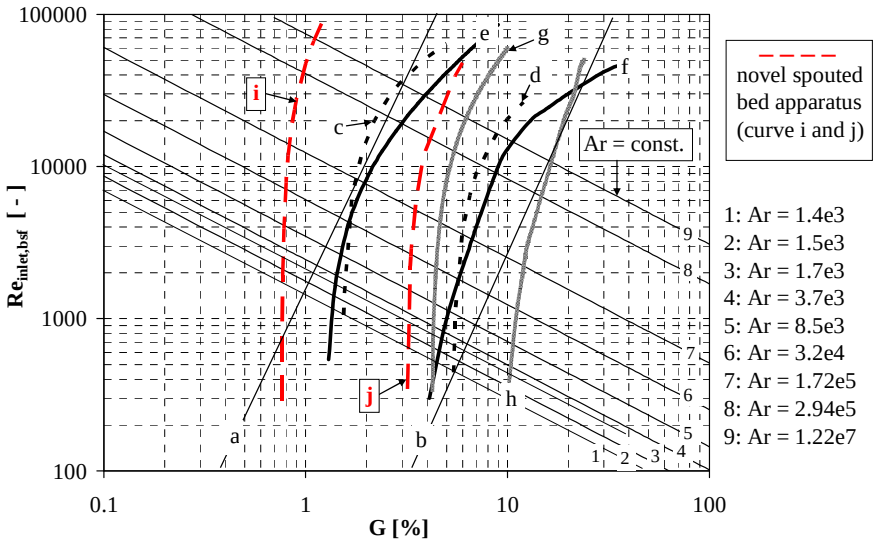

Fig. 3: Comparisons of stable pneumatic domains of different apparatus constructions. Stable operation ranges are located between the curves a and b for a conventional fluidized bed, between the curves c and d for a prismatic spouted bed apparatus with two parallel gas inlets (Piskova (2002)), between the curves e and f for a conical spouted bed apparatus (Olazar (1993)), between the curves g and h for a prismatic spouted bed apparatus with one gas inlet (Mitev (1979)) and between the curves i and j for the novel spouted bed apparatus.

Fig. 5 shows a comparison between a snapshot of the calculated distribution of the granular solid phase in the apparatus with an image of the spouting process. Qualitative good agreement can be observed. Typical zones like the jet zone, the separation zone or the backflow zone can be recognized in the modeling results. In Fig. 6 a qualitative comparison is made between a calculated (by CFD) and an experimentally obtained velocity vector field (by PIV). The circulating particle motion can be recognized from both, PIV measurements and simulation results. Also the calculated velocity magnitude of the solid phase is in good agreement with the PV results. A further perception which can be extracted from the PIV and simulation results is that the particle velocity is much smaller than the gas velocity in the jet zone (respectively 1 – 2 m/s and 20 – 30 m/s).

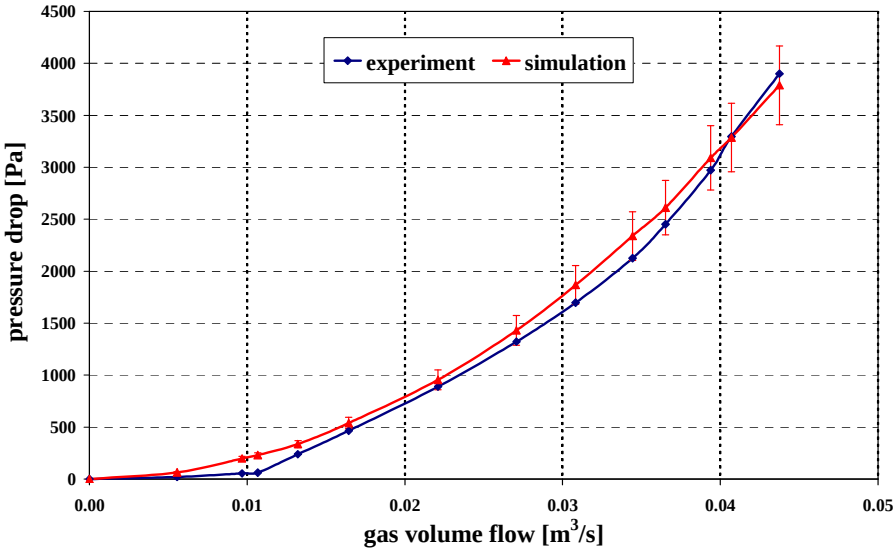

Fig.4: Comparison of experimental and calculated values of the pressure drop of the empty apparatus in dependency of the inlet gas volume flow.

Table 1: Two fluid model, governing equations and simulation settings.

continuity equation for phase q	$\frac{\partial}{\partial t}\left(\alpha_q \rho_q\right)+\nabla\cdot\left(\alpha_q \rho_q \vec{v}_q\right)=\sum_{p=1}^{n}\dot{m}_{pq}$
momentum balance equation for phase q	$\frac{\partial}{\partial t}\left(\alpha_q \rho_q \vec{v}_q\right)+\nabla\cdot\left(\alpha_q \rho_q \vec{v}_q \vec{v}_q\right)=-\alpha_q \nabla p+\nabla\cdot\bar{\bar{\tau}}_q+\sum_{p=1}^{n}\left(\vec{R}_{pq}+\dot{m}_{pq}\vec{v}_{pq}\right)$ $+\alpha_q \rho_q\left(\vec{F}_q+\vec{F}_{lift,q}+\vec{F}_{vm,q}\right)$
stress strain tensor of phase q	$\bar{\bar{\tau}}_q=\alpha_q \mu_q\left(\nabla\vec{v}_q+\nabla\vec{v}_q^{T}\right)+\alpha_q\left(\lambda_q-\frac{2}{3}\mu_q\right)\nabla\cdot\vec{v}_q\bar{\bar{I}}$
gas-solid drag coefficient K_{sl} (Gidaspow et al. (1992))	$\alpha_l>0.8: K_{sl}=\frac{3}{4}C_D\frac{\alpha_s\alpha_l\rho_l\left\lvert\vec{v}_s-\vec{v}_l\right\rvert}{d_s}\alpha_l^{-2.65}$ $\alpha_l\le 0.8: K_{sl}=150\frac{\alpha_s(1-\alpha_l)\mu_l}{\alpha_l d_s^2}+1.75\frac{\rho_l\alpha_s\left\lvert\vec{v}_s-\vec{v}_l\right\rvert}{d_s}$
solid-solid exchange coefficient	$K_{ls}=\frac{3(1+e_{ss})\left(\frac{\pi}{2}+C_{fr,ls}\frac{\pi^2}{8}\right)\alpha_s\rho_s\alpha_l\rho_l(d_l+d_s)^2 g_{0,ls}}{2\pi\left(\rho_l d_l^3+\rho_s d_s^3\right)}\left\lvert\vec{v}_l-\vec{v}_s\right\rvert$
solids shear stress	$\mu_s=\mu_{s,col}+\mu_{s,kin}+\mu_{s,fr}$
kinetic viscosity (Gidaspow et al. (1992))	$\mu_{s,kin}=\frac{10\rho_s d_s\sqrt{\theta_s\pi}}{96\alpha_s(1+e_{ss})g_{0,ss}}\left[1+\frac{4}{5}g_{0,ss}\alpha_s(1+e_{ss})\right]^2$
granular bulk viscosity (Lun et al. (1984))	$\lambda_s=\frac{4}{3}\alpha_s\rho_s d_s g_{0,ss}(1+e_{ss})\sqrt{\frac{\theta_s}{\pi}}$
frictional viscosity (Schaeffer (1987))	$\mu_{s,fr}=\frac{p_s\sin\phi}{2\sqrt{I_{2D}}}$
variation of the coefficient of restitution e_{ss}:	$0.75\le e_{ss}\le 0.9$
variation of the angle of internal friction ϕ	$30°\le\phi\le 45°$

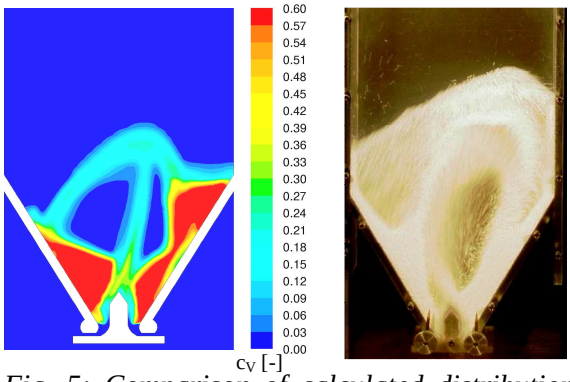

Fig. 5: Comparison of calculated distribution of the solid phase (left) with an image of the spouting process (right); (γ-Al_2O_3-particles, m_{bed} = 1.0 kg, $d_{50,3}$ = 1.75 mm, ρ_s =1040 kg/m^3, gas throughput: 0.036 m^3/s).

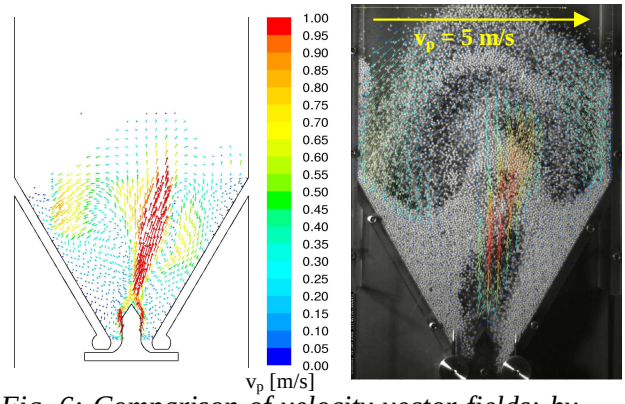

Fig. 6: Comparison of velocity vector fields: by CFD (left) and by PIV (right); (γ-Al_2O_3-particles, m_{bed} = 1.0 kg, $d_{50,3}$ = 1.75 mm, ρ_s =1040 kg/m^3, gas throughput: 0.036 m^3/s).

CONCLUSIONS

In this work the fluidization behavior of a novel spouted bed apparatus with two adjustable gas inlets was investigated. The goal of this work was the identification of the pneumatic operation range by visual observations and by analysis of measured gas phase pressure fluctuations by a FFT. The operation range was depicted in a Re-G-Ar-diagram and compared with other apparatus constructions. Comparison of CFD multiphase modeling results with experiments showed good resemblance regarding the distribution of the granular solid phase in the apparatus as well as velocity vector fields.

NOTATION

A_{bed}	surface of fixed bed, m^2
$A_{gas,inlet}$	area of gas inlet, m^2
Al_2O_3	alumina oxide
Ar	Archimedes number, -
C_D	drag coefficient, -
$C_{fr,ls}$	coefficient of friction, -
c_V	volumetric particle concentration, -
d_s	particle diameter, m
$d_{50,3}$	average particle diameter, m
e_{ss}	coefficient of restitution, -
FFT	fast Fourier transformation
$\vec{F}_{lift,q}$	lift force, N
$\vec{F}_q$	external body force, N
$\vec{F}_{vm,q}$	virtual mass force, N
G	geometric ratio; -
g	acceleration of gravity, m/s^2
$g_{0,ls}$	radial distribution function, -
H_0	initial bed height, m
K_{sl}	solid-liquid momentum exchange coeff., -
$\dot{m}_{pq}$	interphase mass transfer, kg/s
p_s	solids pressure, Pa
q	phase indication subscript, -
$\vec{R}_{pq}$	interphase force, N
$Re_{inlet,bsf}$	Reynolds number at beginning of stable spouting, -
v_{gas}	gas velocity, m/s
v_q	velocity of phase q, m/s
v_p	particle velocity, m/s
α_q	phasic volume fraction, -
α_s	phasic volume fraction of solid phase, -
α_l	phasic volume fraction of liquid phase, -
θ_s	granular temperature, -
λ_q	granular bulk viscosity, $Pa \cdot s$
μ_q	shear viscosity, $Pa \cdot s$
μ_s	solids shear stress, $Pa \cdot s$
$\mu_{s,col}$	collisional viscosity, $Pa \cdot s$
$\mu_{s,kin}$	kinetic viscosity, $Pa \cdot s$
$\mu_{s,fr}$	frictional viscosity, $Pa \cdot s$
ν_{gas}	kinematic gas viscosity, m^2/s
ρ_{gas}	gas density, kg/m^3
ρ_s	particle density, kg/m^3
ρ_q	density of phase q, kg/m^3
σ	standard deviation, m
$\bar{\bar{\tau}}_q$	stress strain tensor of phase q, -
Φ	angle of internal friction, °
ΔP	pressure drop, Pa

REFERENCES

Čatipović, N. M., Jovanović, G. N., Fitzgerad, T. J.: AIChE J., (1978), pp. 543-547.

Goldschmidt, M. J. V., Beetstra, R., Kuipers, J. A. M.: Powder Technology, (2004), 142(1), pp. 23-47.

Gidaspow, D., Bezburuah, R., Ding, J.: Fluidization 7, (1992), Proceedings of the 7th Engineering Foundation Conference on Fluidization, pp. 75-82.

Gryczka, O., Heinrich, S., Miteva, V., Deen, N.G., Kuipers, J.A.M., Jacob, M., Mörl, L.: Chem. Eng. Sci. (2008) 3, 791-814.

Hatano, S., Kaneko, K., Oura, Y., Mori, S.: Funtai Kogaku Kaishi, (2004), 41(8), pp. 586-591.

Jacob, M., Piskova, E., Mörl, L., Krueger, G., Heinrich, S., Peglow, M., Ruempler, K. H.: World Congress of Chemical Engineering, 7th, Glasgow, United Kingdom, July 10-14, (2005), 86855/1-86855/10.

Kfuri, C. R., Freitas, L. A. P.: Drying Technology, (2005), 23(12), pp. 2369-2387.

Kmiec, A., Kucharski, J., Mielczarski, S.: Investigations of Drying Kinetics of Coal in a Spouted Bed Dryer, Inzynieria i Aparatura Chemiczna 33 (1994) 3, pp. 17-19.

Kojouharov K.: Ph.D. Thesis, Otto-von-Guericke-Universität Magdeburg (2004).

Lun, C.K.K., Savage, S.B., Jeffrey, D.J., Chepurniy, N.: J. Fluid Mech., (1984), 140: pp. 223-256.

Markovski, A., Kaminski, W.: Can. J. Chem. Eng. 61, (1983), pp. 377-381.

Mitev, D. T.: (russ.) Ph.D. Thesis, LTI Leningrad (1967).

Mitev. D.T.: (russ.), Habilitation, LTI Leningrad (1979).

Mörl, L., Krüger, G., Heinrich, S., Ihlow, M., Jordanova, E.: Deutsche Patentanmeldung 10004939.7, Patentinhaber: Glatt GmbH, (2001).

Olazar, M., San Jose, M. J., Aguayo, A. T., Arandes, J. M., Bilbao, J.: Ind. Eng. Chem. Res. 31, (1992), pp. 1784-1792.

Olazar, M., San Jose, M. J., Aguayo, A. T., Arandes, J. M., Bilbao, J.: Ind. Eng. Chem. Res., 32, (1993), pp. 1245-1250.

Piskova, E.: Ph.D. Thesis, Otto-von-Guericke-Universität Magdeburg (2002)

Schaeffer, D.G.: J. Diff. Eq., (1987), 66: pp. 19-50.

Van Wachem, B. G. M., Schouten, J. C., Krishna, R., Van den Bleek, C. M.: Chemical Engineering Science, 54(13-14), (1999), pp. 2141-2149.

Wu, Z. and Mujumdar, A.S.: Drying Technology, (2007), 25: pp. 59–74.

ACKNOWLEDGMENT

This work was supported by the DFG-Graduiertenkolleg 828, ‘Micro-Macro-Interactions in Structured Media and Particle Systems’. The authors gratefully thank for funding through this Ph.D. program.